DEVELOPMENTAL DYNAMICS 238:632–640, 2009

TECHNIQUES

MicroCT for Developmental Biology: A Versatile Tool for High-Contrast 3D Imaging at Histological Resolutions

Brian D. Metscher*

Understanding developmental processes requires accurate visualization and parameterization of three-dimensional embryos. Tomographic imaging methods offer automatically aligned and calibrated volumetric images, but the usefulness of X-ray CT imaging for developmental biology has been limited by the low inherent contrast of embryonic tissues. Here, I demonstrate simple staining methods that allow high-contrast imaging of embryonic tissues at histological resolutions using a commercial microCT system. Quantitative comparisons of images of chick embryos treated with different contrast agents show that three very simple methods using inorganic iodine and phosphotungstic acid produce overall contrast and differential tissue contrast for X-ray imaging at least as high as that obtained with osmium. The stains can be used after any common fixation and after storage in aqueous or alcoholic media, and on a wide variety of species. These methods establish microCT imaging as a useful tool for comparative developmental studies, embryo phenotyping, and quantitative modeling of development. ***Developmental Dynamics 238: 632–640, 2009.*** **© 2009 Wiley-Liss, Inc.**

Key words: microCT; X-ray computed tomography; three-dimensional imaging; chick; embryonic development; contrast agents

Accepted 9 December 2008

INTRODUCTION

The need for three-dimensional (3D) representations of developing embryos is as old as embryology itself, and our modern genomic, functional, mutational, and quantitative approaches to studying developmental processes are no less dependent on accurate knowledge of normal and affected tissues and structures (Dickinson, 2006). This requires size-calibrated 3D images that preserve the volumetric relationships within the original specimen. Confocal microscopic methods provide such images for samples that are no thicker than a few hundred microns and usually fluorescence-labeled (Wanninger, 2007), and histological reconstructions from serial sections are extremely labor-intensive and give uneven results. Episcopic (Weninger et al., 2006) and other block-face (Ewald et al., 2002; Tyszka et al., 2005) microscopic imaging techniques provide automatically aligned high-resolution serial-slice image stacks of embedded samples, but the sample is destroyed in the imaging process. For embryo-size samples, tomographic imaging methods are the most natural candidates for nondestructive volumetric imaging.

X-ray microtomography (microCT) is already widely used in studies of mineralized tissues (e.g., Neues et al., 2007; Stauber and Müller, 2008; Vasquez et al., 2008), and it has been effectively used in quantitative studies of variation (Hallgrimsson et al., 2007) and of development (Parsons et al., 2008). The applications of other tomographic methods, particularly micro-MRI (Jacobs et al., 2003; Ruffins et al., 2007) and optical projection tomography (Kerwin et al., 2004; Sharpe, 2004), have been demonstrated convincingly, but the use of X-ray–based tomographic imaging

Additional Supporting Information may be found in the online version of this article.

Department of Theoretical Biology, University of Vienna, Vienna, Austria
***Correspondence to: Brian D. Metscher, Department of Theoretical Biology, Althanstrasse 14, University of Vienna, Vienna 1090, Austria. E-mail: brian.metscher@univie.ac.at**

DOI 10.1002/dvdy.21857
Published online 16 February 2009 in Wiley InterScience (www.interscience.wiley.com).

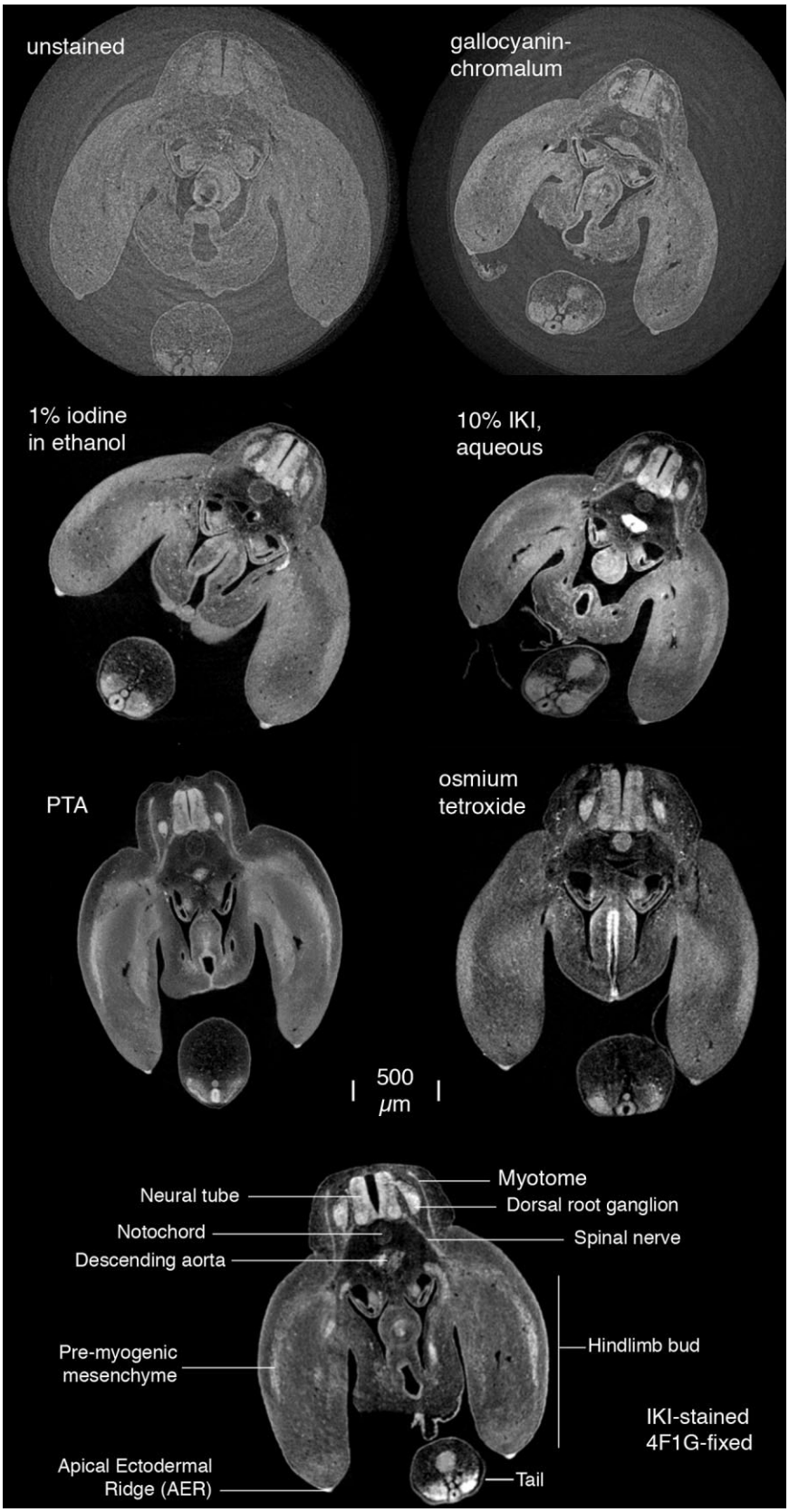

Fig. 1.

has been constrained by the low intrinsic X-ray absorption of unmineralized tissue and the lack of established contrast agents. Phase contrast enhancement of X-ray images (Betz et al., 2007), while useable on unstained material, is much more useful for objects with distinct edges, rather than the softer gradients characteristic of embryos. Three-dimensional X-ray microscopy has been used to image subcellular structures (Larabell and Le Gros, 2004; Le Gros et al., 2005), but resolutions of tens of nanometers require a synchrotron source and a field of view too small to be of general utility to organismal developmental research.

To date, the most successful contrast stain used for microCT imaging of soft tissues and embryos is osmium tetroxide (Johnson et al., 2006; Bentley et al., 2007). The K-shell energy of osmium (73.9 keV) and its known tissue binding properties (Kiernan, 1990) make osmium tetroxide a natural candidate for an X-ray contrast stain. And although the staining is already available in any institution with an EM facility, its tissue penetration is limited (Hayat, 1970), it does not work well on tissues that have been preserved in alcohol, and osmium is volatile, toxic, and expensive to purchase and to dispose of.

This work presents quantitative comparisons of contrast in microCT images of chick embryos treated with several very simple contrast stains. To illustrate the usefulness of microCT for developmental biology, high-contrast, true-volume images of chick em-

Fig. 1. Comparison of several contrast stains. Virtual sections through the hindlimb buds of stage 24 chick embryos. For illustration, each volume image was re-sliced arbitrarily along the hindlimb proximodistal axis to show, among other structures, the spinal ganglia, spinal nerves, myogenic mesenchyme, and apical ectodermal ridge. The images were processed for illustration only by rotating, cropping, and adjusting the window and level values (brightness and contrast). The reconstructed voxel size in these images after 2 × 2 binning is 4.6 μm (5.1 μm for the osmium and IKI/4F1G images), giving a practical spatial resolution limit of approximately 12 μm. All slices are one voxel thick and are shown at the same scale. The 10% IKI image shows saturated brightness in the descending aorta most likely due to intense staining of blood trapped during fixation.

bryos are presented showing developing structures and tissues at spatial resolutions comparable to low-power light micrographs of histological sections.

RESULTS AND DISCUSSION

Soft-tissue contrasts produced by several stains are illustrated in Figure 1, and quantitative comparisons of the raw tomographic images are given in Figure 2. Because computed tomographic CT values represent linear X-ray absorption coefficients (Kalender, 2005), the voxel grayscale values can be used as a linear measure of relative absorption at different points in the sample for a given X-ray source spectrum. Using a simple common reference material—the alcohol in which each sample was scanned—directly comparable measures of absorption for differently stained tissues were obtained.

Unstained embryonic tissue in alcohol gives discernable X-ray contrast, but the pixel brightness distributions of the object and background medium overlap considerably (Fig. 2). All contrast is due to intrinsic differences in tissue density and composition, and overall X-ray contrast is low, around 30% above that of ethanol. Contrast was even lower for unstained samples in water (not shown), possibly because of the condensing effect of alcohol dehydration on proteins (Kiernan, 1990).

Gallocyanin-chromalum, a histological stain for cell nuclei (Presnell and Schreibman, 1997), appears to impart X-ray contrast to tissues according to their native cell densities (Fig. 1). It gave a clearer overall contrast between object and background than unstained tissue, but not enough difference to allow complete exclusion of background by raising the limit of pixel values displayed as black (i.e., the lower limit of the brightness window; Fig. 2, histogram).

The two inorganic iodine stains gave results similar to each other, and both are extremely simple to prepare and use (Table 1). Penetration into tissues was rapid, and contrast imparted to various tissues is excellent. Tissues stored in alcohol stained well with 1% iodine in absolute ethanol (I2E) or methanol (I2M) after being dehydrated to pure alcohol. Iodine potassium iodide (IKI, one formulation of Lugol's solution) works well on fixed tissues that are still in aqueous medium. A 10% dilution of IKI in water was found to work as well as pure IKI but with less tissue shrinkage. IKI-stained samples could also be scanned in water (not shown), and the staining was stable for at least a few months in samples stored in ethanol.

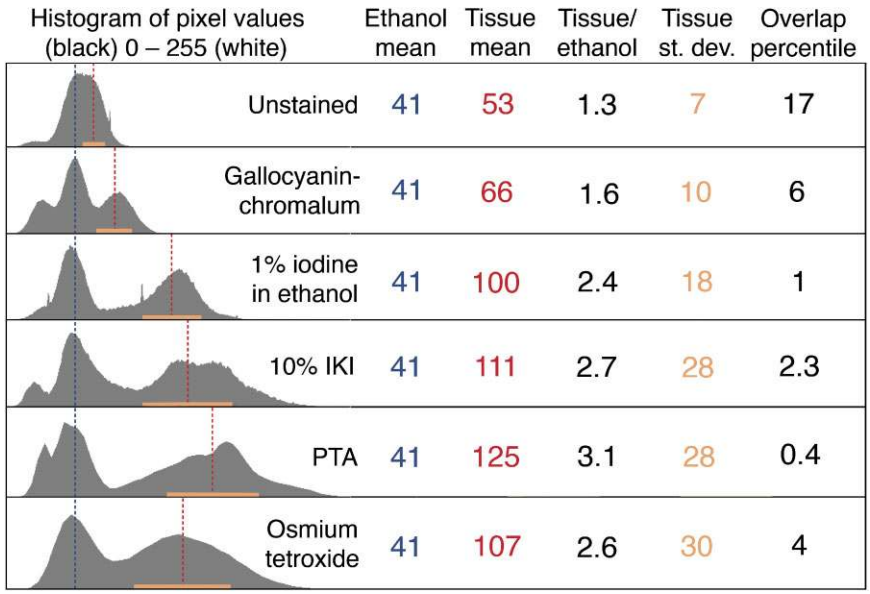

Fig. 2. Quantitative measures of contrast for the staining methods illustrated in Figure 1. For analysis, raw reconstructed tomographic sections were used before any processing or re-slicing. A histogram for each stain shows the distribution of pixel grayscale values, on a relative linear scale. Each graph has been scaled to the same mean for the ethanol background peak (blue dashed line). The mean of the object pixel distribution after scaling is marked by a vertical red dashed line, and the orange bar indicates the width of one standard deviation above and below the mean. (Medians for all distributions were nearly equal to the means.) The smaller peak to the left of the alcohol peak in some histograms represents the polypropylene in the sample holders, depending on how much of the plastic appeared in the selected slice.

Phosphotungstic acid staining is equally simple (Table 1), and also produces excellent contrast among different tissues. The staining is stable for at least several months, but penetration is much slower than iodine: chick embryos later than approximately stage 24 required overnight or longer. PTA is especially suitable for Bouin- or formalin-fixed material stored in 70% alcohol. Chick embryos fixed in Glyo-Fixx (glyoxal-based) and stored in methanol worked well also. Phosphomolybdic acid was tested on a few samples and gave similar results to PTA, but this stain was not investigated fully, because PTA is at least as widely used in histology and EM labs (Hayat, 1970).

All the stains imparted clear contrast to neural tissues and to denser aggregations such as premyogenic mesenchyme and the apical ectodermal ridge. Epithelia can be distinguished from mesenchyme, and some detail can be seen within the neural tube and other structures.

Osmium staining was tested alongside PTA and IKI on chick embryos fixed in 3.7% formaldehyde, 1% gluteraldehyde in phosphate buffer (4F1G; McDowell and Trump, 1976). This fixation gave excellent tissue preservation with all three stains. The other stains tested here gave X-ray images at least as good as those obtained with osmium (Fig. 1), and they are simpler and more versatile. The finer detail in the osmium specimen is due in large part to the fixative (4F1G instead of formalin), which, in combination with osmium tetroxide postfixation, resulted in less shrinkage than the other treatments.

To quantify the differences among staining methods, the ratio of mean object level to mean ethanol background level was used as a simple measure of separation of signal from noise (Fig. 2). Because all samples use the same background medium, this ratio is also directly proportional to

TABLE 1. Useful Contrast Stains for Soft-Tissue MicroCT

Contrast stain	Gallocyanin-chromalum	IKI (Lugol's) iodine potassium iodide	I2E, I2M alcoholic iodine	PTA phosphotungstic acid	Osmium tetroxide
Sample fixation[a] and storage	NBF, Bouin's; still in aqueous medium	NBF, 4F1G; still in aqueous medium	Any fixation; ethanol- or methanol-preserved specimens	NBF, Bouin's, 4F1G; aqueous or alcoholic storage	4F1G or other EM fix; not alcohol-dehydrated
Stain solution[b]	Gallocyanin-chromalum 5% (w/v) in water. Boil to dissolve, cool and filter. Stable for 1-2 weeks.	1% (w/v) iodine metal (I_2) + 2% potassium iodide (KI) in water. Stable for months. Dilute to 10% in water just before use.	1% (w/v) iodine (I_2) in 100% ethanol (I2E) or methanol (I2M). Stable for months.	1% (w/v) PTA in water. Mix 30% PTA solution, 70% abs. ethanol Stable for months.	1-2% OsO_4 in phosphate buffer
Staining procedure	Wash samples in water. Stain overnight. Wash in water. Dehydrate to ethanol.	Samples in aqueous solution. Stain 30 min to overnight. Wash in water. Dehydrate to ethanol.	Samples in 100% alcohol. Stain 30 min to overnight. Wash in alcohol.	Samples in 70% ethanol. Stain 2 hr to overnight. Wash in 70% ethanol. Scan in 70-100% ethanol.	Stain 1-2 hr. Wash in phosphate buffer. Dehydrate to ethanol.
Advantages	Demonstrates cell densities and individual cells. Possibly useful as counterstain.	Rapid and deep penetration. Excellent contrast. Cheap, simple, nontoxic. Versatile, robust.		Excellent contrast. Stable stain. Sharp tissue differentiation.	Combines readily with EM. High contrast. Can be used on resin blocks.
Limitations	Low overall contrast.	May overstain some mineralized tissues. Intensity and permanence may vary with different samples preparations.		Slow tissue penetration, limited to a few millimeters.	Toxic, expensive disposal. Limited penetration. Not useful for alcohol-stored tissues.

[a]Fixatives: NBF: neutral-buffered formalin (3.7% formaldehyde in 0.1M phosphate buffer, pH 7.0); 4F1G: 3.7% (or 4%) formaldehyde, 1% gluteraldehyde in 0.1M phosphate buffer; Glyo-Fixx (Thermo Electron Corp. Shandon Glyo-Fixx) or Prefer (Anatech Ltd.): glyoxal-based formalin substitute.

[b]Stains: gallocyanin-chromalum: Chroma 1A 458 (Pressnell and Schreibman, 1997); iodine: Sigma 20,777-2 ; potassium iodide: Sigma 207969; phosphotungstic acid: Mallinckrodt 2824.

the ratio of stained tissue level to unstained tissue level. The means measure overall stained-tissue contrast for this X-ray source (tungsten at 40 kV), and the dispersion of object pixel values reflects the range of brightness levels among stained tissues. Because outlying points in the brightness distribution are important for differentiating among tissue features, a root-mean-square measure like standard deviation is more appropriate here than a linear nonparametric measure such as interquartile range. It is important to note that this is a measure of the difference between two absorbing materials and not a measure of image background noise.

A desirable feature in a micrograph is the possibility of setting the brightness level and window so that background is eliminated. A simple nonparametric measure of object-background separation is given by the overlap percentile between the two distributions (Fig. 2, last column). This is calculated simply as the percentile score at which the left-tail percentile object distribution is equal to the right-tail percentile background distribution. This measure is independent of the number of pixels in either sampled distribution, but it does require separate sampling of the two distributions. It gives the fraction of pixels within the object that have a 50% or greater probability of having their brightness value due to absorption by the intercalating medium rather than object. An image display window function with its lower bound set at this point will eliminate all but that percentage of background pixels, at a cost of the same percentage of object pixels. This may or may not correspond to the optimum window for overall image quality, but it is a consistent quantitative measure of object and medium separation in images of an object in an absorbing medium. The precision with which the overlap percentile can be estimated is determined by the percentile differences between adjacent histogram bins (hence, the different precisions for the overlap percentiles given in Fig. 2).

To demonstrate the usefulness of these methods in embryology research, normal chick embryos of several stages were stained and imaged at different magnifications (Figs. 3–7). At stage 12, the virtual sections and partial volume renderings may be more informative than the complete outward view (Fig. 3, top). The invaginating otic placode and neural crest are represented clearly with both IKI and gallocyanin staining (Figs. 3, 4), and the image resolution, even after 2 × 2 pixel binning, is sufficient to show individual cells.

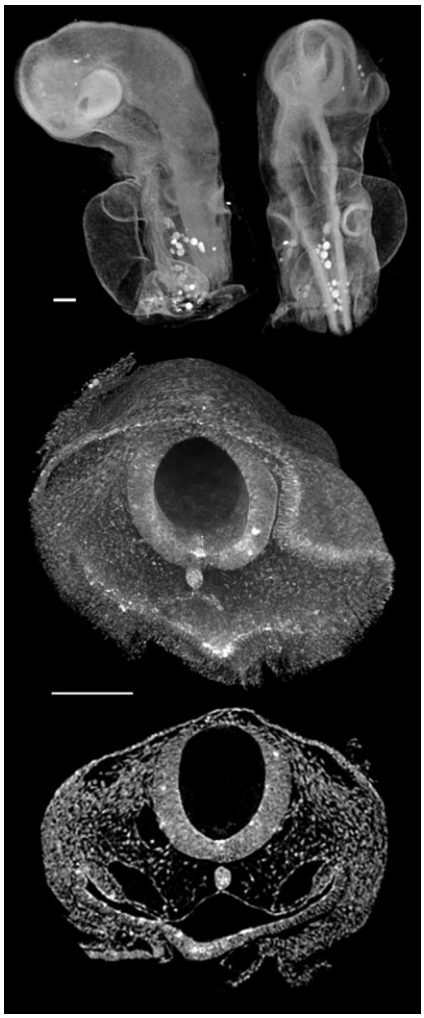

Fig. 3. Stage 12 chick embryo stained with 10% IKI (iodine potassium iodide). Top: A volume rendering of the head shown at two different angles. Reconstructed cubic voxel size is 3.5 μm after 2 × 2 binning. Center: Higher magnification scan of the same stage (0.97 μm voxels), showing an oblique cutaway volume rendering. View is from anterior, and the virtual cut passes through the otic placode on the right and posterior to it on the left, where neural crest cells can be seen. Bottom: A single virtual section through the same volume image. Scale bars = 100 μm.

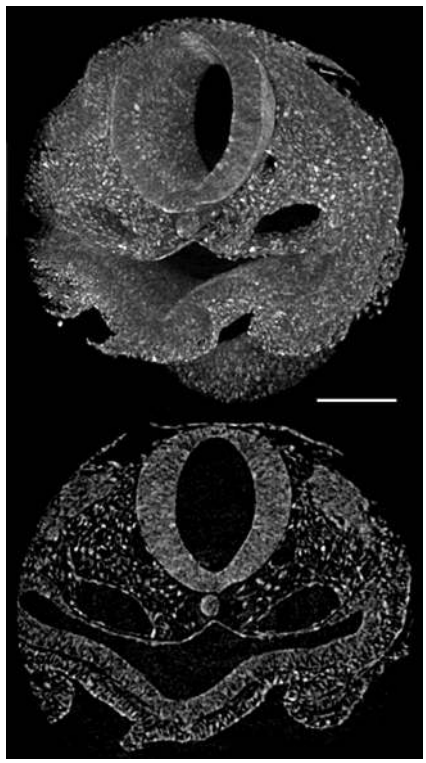

Fig. 4. Stage 12 chick embryo stained with gallocyanin-chromalum. Individual cells are clearly distinguishable, although no specific tests were performed to confirm that the X-ray contrast is restricted to cell nuclei. Tissue that took up less of the stain, especially undifferentiated mesenchyme, shows little or no X-ray contrast above the background and, therefore, appears as dark in a single (one voxel thick) section. Voxel size, 0.99 μm. Scale bar = 100 μm.

The volume rendering of a stage 14 chick head (Fig. 5 and Supp. Video, which is available online) shows the heart loop, the developing regions of the brain, the rhombomeres, the otic vesicles, and the cranial nerves (Supp. Video S1, which is available online). The reconstructed images preserve the original shapes and positions of tissues and organs in the scanned sample. CT imaging avoids distortions due to realignment of separately imaged sections, but any distortion or shrinkage due to sample fixation or dehydration must still be accounted for just as in histology or any other imaging method.

At stage 24, the placement of the cranial nerves is clearly shown (Fig. 6 and Supp. Video), as are the posterior spinal nerves and ganglia. As with most tissue stains, PTA and iodine give clearer contrast to differentiated tissues than to embryonic mesenchyme. Even so, the premyogenic mesenchyme in the hindlimbs is demonstrated effectively by both stains (Figs. 1, 6).

Developmental Dynamics

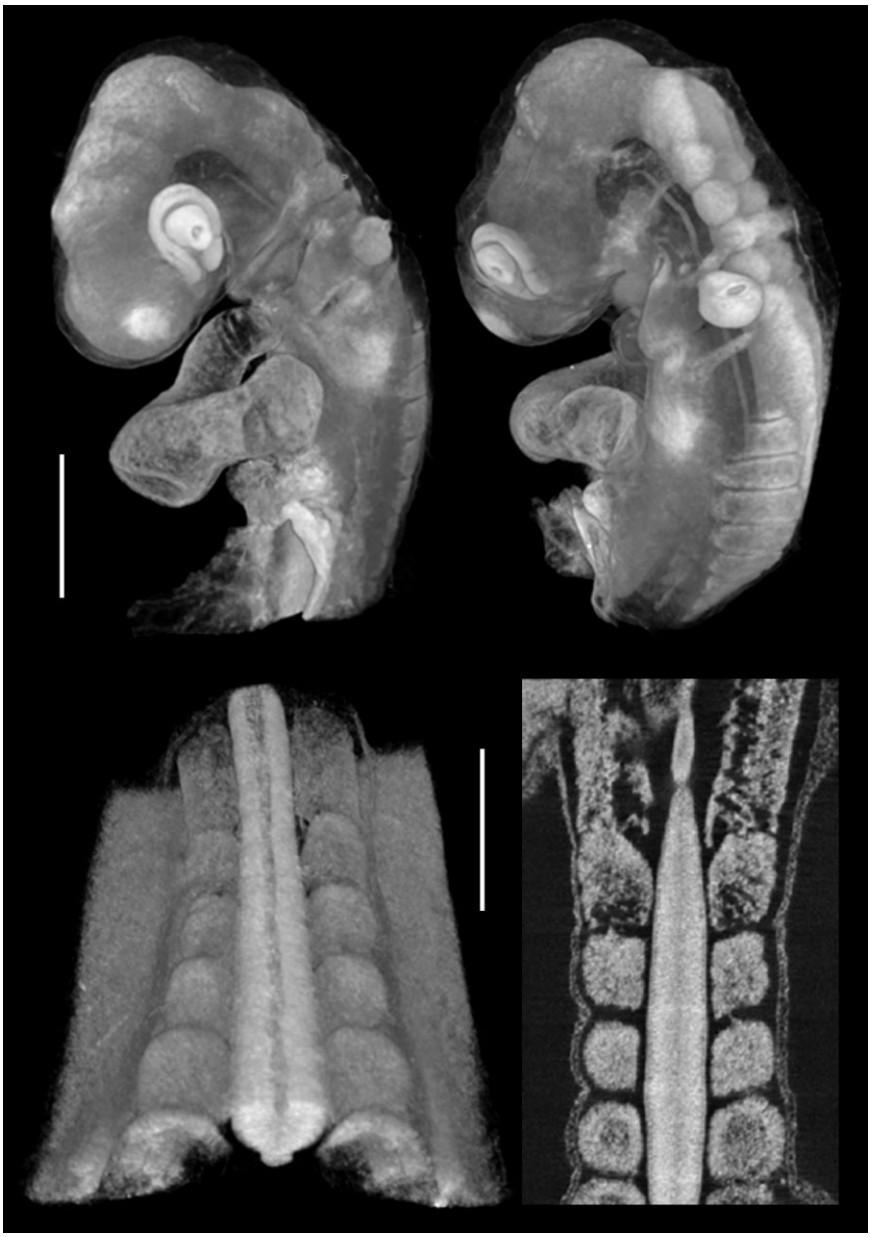

Fig. 5. Stage 14 chick embryo, PTA stained. Top: Volume rendering of the head and pharyngeal region, 4.9 μm voxels. The heart loop, otic vesicles, cranial nerves, and rhombomeres are clearly visible. Bottom: Region of somitogenesis, volume rendering and single horizontal virtual section. Posterior is toward the top of the figure. Voxel size, 0.99 μm. Scale bars: top = 500 μm, bottom = 100 μm.

The stains tested here are similar in their overall contrast enhancement, and none of them is tissue-specific. PTA is acidic in solution, and may result in decalcification or other chemical changes to stained tissues; further tests are needed to determine these effects. Iodine has been observed to overstain some mineralized tissues, giving areas of saturation in X-ray images. Both stains tend to bind heavily to yolk, which can be a difficulty when imaging embryos of some species.

The staining methods are not species-specific, and are predicted to give useful results for almost any model or nonmodel animal. A few samples of mouse, *Xenopus*, and zebrafish embryos have been tested with PTA and I2E, and the preliminary results (not shown) indicate that the presented staining methods will give useful results with other model species. In addition to model species embryos, one or another of these stains has been used successfully on samples from no fewer than 20 different species in five chordate classes and four invertebrate phyla. It is anticipated that these contrast methods will find broad applications in various areas of animal research.

By using very simple contrast stains, microCT can be used to make high-contrast, high-resolution, true-3D images of embryonic and other unmineralized tissues. Because the imaging is nondestructive, it can be combined with other analysis methods such as transmission electron microscopy or histology, and it can be used on rare or irreplaceable samples, such as rare embryos or old museum specimens. The methods presented can be used for specimens in liquid media or embedded in resins, with no need for drying. Tomographic images are inherently volumetric and automatically aligned and size-calibrated, so they are directly useful for quantitative studies and theoretical modeling of development. All of the embryos imaged for this demonstration are of unperturbed phenotypes, but the range of applicability of these methods to studies of natural and artificial genetic variants, experimentally manipulated embryos, and different species are not difficult to envisage.

EXPERIMENTAL PROCEDURES

The self-contained X-ray microtomography system used in this work is model MicroXCT from Xradia Inc., Concord, CA (www.xradia.com). This scanner uses a Hamamatsu L9421-02 tungsten X-ray source with an anode voltage between 20 and 90 kV, power between 4 and 8W, and a spot size of 5 to 8 μm. This scanner's configuration allows fields of view from 5 mm down to less than 500 μm. For the demonstrations presented here, the beam was filtered only by the beryllium window of the X-ray source housing. The X-ray projection image is formed on a scintillator crystal, made in-house by Xradia. The optical emissions of the scintillator is then imaged by a Nikon microscope objective lens onto a CCD camera cooled to −55°C to reduce dark noise. The optical imaging of the scintillator allows a final magnification independent of the geometric magnification of the X-ray projection imaging, and a final image resolution

Developmental Dynamics

that is not limited by the X-ray source spot size. Several different optical objective lenses allow selection of the final magnification, while adjustments to the source-sample and sample-detector distances can be used to change the geometric magnification of the sample image on the scintillator.

Projection images are collected and tomographic slices reconstructed by Xradia's supplied software running on a dedicated Dell Precision 490 computer. The system automatically subtracts a background image from each projection, and the reconstruction program uses a ring-artifact-reduction utility. Projection images were collected as 1,024 × 1,024-pixel frames and binned 2 × 2 during reconstruction, partly to reduce noise and partly to reduce file size, resulting in image blocks of 512 × 512 × 512 voxels (actually slightly less due to clipping outside the cone shape of the X-ray beam). The 3D images were stored as 8-bit grayscale image stacks, requiring approximately 130 MB of disk space if saved in TIFF format. It is possible to reconstruct and use the full-size images, but each volume image is over 1 GB in size and the computing can become cumbersome.

For the contrast comparisons in Figures 1 and 2, a set of stage 24 chick embryos (Hamburger and Hamilton, 1992) were fixed in 10% phosphate-buffered formalin and stained overnight in 10% IKI, 1% iodine in ethanol, 0.3% PTA in 70% ethanol, or 5% gallocyanin-chromalum in water (details are given in Table 1). Each stain was washed out with its respective solvent, and all samples were dehydrated to ethanol. Unstained samples were simply fixed and dehydrated to ethanol for scanning. A second set of embryos was fixed in 4F1G (3.7% formaldehyde + 1% gluteraldehyde in 0.2 M phosphate buffer) overnight for staining with osmium (1% osmium tetroxide in 0.05% phosphate buffer for 2 hr), IKI, and PTA.

The scans used in this analysis were made with a source voltage of 40 kV (40 keV maximum X-ray energy), with a 20-sec exposure every 0.25° over 180° rotation. All samples were scanned in ethanol in 200-μl polypropylene pipette tips, using the ×4 objective lens in the MicroXCT, and all at the same source-sample and sample-detector distances (40 mm and 16 mm, respectively). Comparable slices were taken directly from each reconstructed 3D image, before any further processing, for analysis. The signal and background of each image were sampled by outlining most of the alcohol-filled space or the embryo tissue using the lasso tool in ImageJ 1.40, and the object and background regions were analyzed by using the histogram tool to obtain numerical data and summary statistics for each pixel brightness distribution. The distributions were normalized to the same mean background value (which represents a CT value for ethanol). The location and dispersion of CT values of the stained tissues could then be compared directly. Histograms of the actual sampled data were produced using Plot 0.997, and the final chart was assembled with Adobe Illustrator CS3.

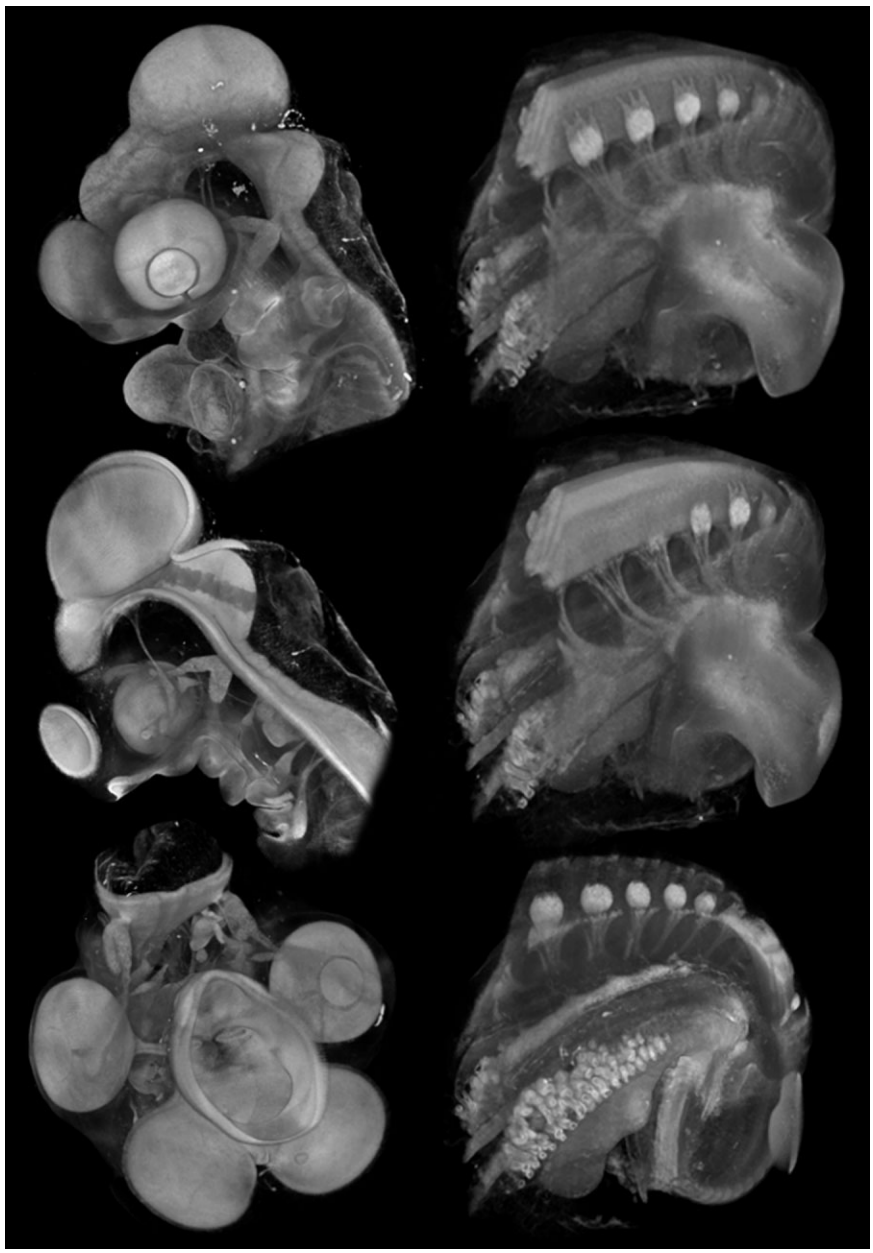

Fig. 6. Stage 24 chick embryos. Left: IKI-stained head showing brain and cranial nerves (9.5 μm voxels). Bottom left: inferior view of the brain, eyes, and cranial nerves. Right: PTA-stained pelvic region showing hindlimb buds, spinal nerves and ganglia, and mesonephros (4.6 μm voxels). While these stains are not tissue-specific, they do allow clear differentiation among structures.

Developmental Dynamics

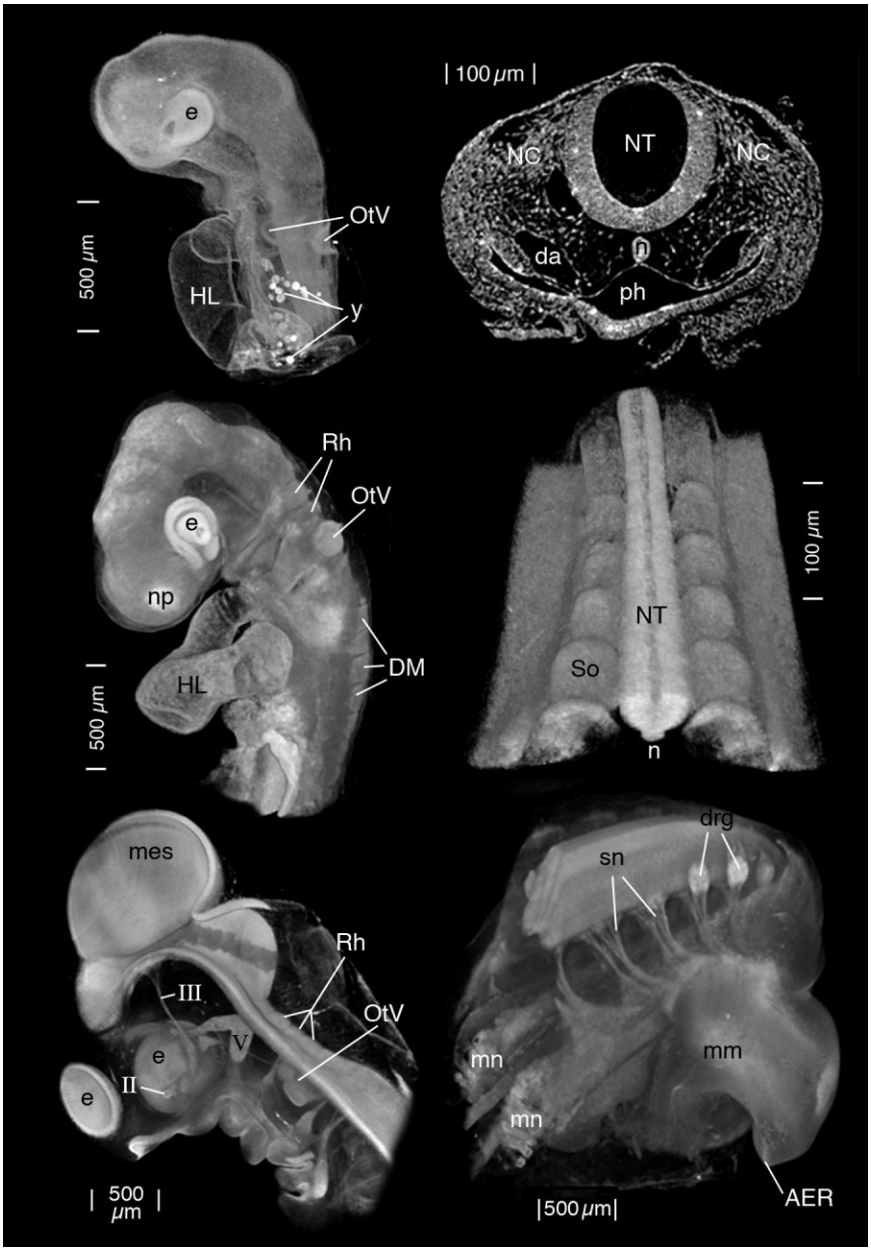

Fig. 7. Guide to some features visible in Figures 3–6. AER, apical ectodermal ridge; da, dorsal aorta; DM, derma-myotomes; drg, dorsal root ganglia; e, eye; HL, heart loop; mes, mesencephalon; mm, premyogenic mesenchyme; mn, mesonephros; n, notochord; NC, neural crest; NT, neural tube; ph, pharynx; np, nasal placode; OtV, otic vesicle; Rh, rhombomeres; sn, spinal nerves; So, somite; y, yolk granules; II, optic nerve; III, oculomotor nerve; V, trigeminal nerve.

To illustrate the different contrast stains (Fig. 1), virtual re-sliced images were processed from the scans used for the analysis presented in Figure 2. The display levels were adjusted in Photoshop CS3 to show the contrasts and clarity obtainable with each stain. For all but the osmium scan, the source-sample distance was 40 mm and the sample-detector distance was 16 mm. The osmium sample was scanned with the source at 60 mm to give a slightly larger field of view, because the 4F1G-fixed, osmicated sample shrank less than the formalin-fixed samples.

Scans of other chick embryos were made similarly, but using combinations of source and detector distances and objective magnifications appropriate to the different specimen sizes. Samples were scanned in ethanol, although other liquids can be used. To minimize the amount of fluid surrounding the specimen, each sample was placed in either a 0.2-ml PCR tube or a micropipette tip (both are polypropylene, with 200- to 300-μm-thick walls). For smaller embryos, a micropipette tip (200 or 1,000 μl) was flame-sealed at the tip, filled with alcohol, and agitated to remove bubbles. The sample was simply placed in the alcohol and allowed to sink, then pressed gently into the conical cavity to brace it against rotation during scanning. The sample was easily removed without damage by cutting off the tip below it and washing it out. Larger samples were placed in a PCR tube full of alcohol and held in place by a small piece of alcohol-soaked sponge. The tube could then be inverted and mounted on a sample holder (provided with the microCT scanner) with adhesive putty (e.g., UHU Patafix).

Reconstructions of samples stained with heavy metals are sometimes improved by adjusting the beam-hardening constant used by the reconstruction program. This factor helps account for greater attenuation of lower energy ("softer") X-rays as the broadband beam traverses the sample and can remove some "shadow" effects in the reconstructed slices. The reconstructions of PTA-stained embryos shown in Figure 6 used a beam-hardening constant of 0.6 instead of the default value of 0.

Volume images were displayed using the software provided by Xradia (TXM3DViewer), which allows exporting of virtual section images as well as volume projections and movies. The rendered volume images can be adjusted in size, orientation, windowing, and transparency.

ACKNOWLEDGMENTS

The author thanks Prof. Gerd Müller for advice and guidance, and the University of Vienna for supporting this research.

REFERENCES

Bentley MD, Jorgensen SM, Lerman LO, Ritman EL, Romero JC. 2007. Visualization of three-dimensional nephron structure with microcomputed tomography. Anat Rec (Hoboken) 290:277–283.

Betz O, Wegst U, Weide D, Heethoff M, Helfen L, Lee WK, Cloetens P. 2007. Imaging applications of synchrotron X-ray phase-contrast microtomography in biological morphology and biomaterials science. I. General aspects of the technique and its advantages in the analysis of millimetre-sized arthropod structure. J Microsc 227:51–71.

Dickinson ME. 2006. Multimodal imaging of mouse development: tools for the postgenomic era. Dev Dyn 235:2386–2400.

Ewald AJ, McBride H, Reddington M, Fraser SE, Kerschmann R. 2002. Surface imaging microscopy, an automated method for visualizing whole embryo samples in three dimensions at high resolution. Dev Dyn 225:369–375.

Hallgrimsson B, Lieberman DE, Liu W, Ford-Hutchinson AF, Jirik FR. 2007. Epigenetic interactions and the structure of phenotypic variation in the cranium. Evol Dev 9:76–91.

Hamburger V, Hamilton HL. 1992. A series of normal stages in the development of the chick embryo. 1951. Dev Dyn 195: 231–272.

Hayat MA. 1970. Principles and techniques of electron microscopy: biological applications. New York: Van Nostrand Reinhold.

Jacobs RE, Papan C, Ruffins S, Tyszka JM, Fraser SE. 2003. MRI: volumetric imaging for vital imaging and atlas construction. Nat Rev Mol Cell Biol Suppl:SS10–SS16.

Johnson JT, Hansen MS, Wu I, Healy LJ, Johnson CR, Jones GM, Capecchi MR, Keller C. 2006. Virtual histology of transgenic mouse embryos for high-throughput phenotyping. PLoS Genet 2:e61.

Kalender WA. 2005. Computed tomography: fundamentals, system technology, image quality, applications. Erlangen: Publicis Corporate Publishing. 304 p.

Kerwin J, Scott M, Sharpe J, Puelles L, Robson SC, Martinez-de-la-Torre M, Ferran JL, Feng G, Baldock R, Strachan T, Davidson D, Lindsay S. 2004. 3 dimensional modelling of early human brain development using optical projection tomography. BMC Neurosci 5:27.

Kiernan JA. 1990. Histological and histochemical methods: theory and practice. Oxford: Pergamon Press.

Larabell CA, Le Gros MA. 2004. X-ray tomography generates 3-D reconstructions of the yeast, saccharomyces cerevisiae, at 60-nm resolution. Mol Biol Cell 15: 957–962.

Le Gros MA, McDermott G, Larabell CA. 2005. X-ray tomography of whole cells. Curr Opin Struct Biol 15:593–600.

McDowell EM, Trump BF. 1976. Histologic fixatives suitable for diagnostic light and electron microscopy. Arch Pathol Lab Med 100:405–414.

Neues F, Goerlich R, Renn J, Beckmann F, Epple M. 2007. Skeletal deformations in medaka (Oryzias latipes) visualized by synchrotron radiation micro-computer tomography (SRmicroCT). J Struct Biol 160:236–240.

Parsons TE, Kristensen E, Hornung L, Diewert VM, Boyd SK, German RZ, Hallgrimsson B. 2008. Phenotypic variability and craniofacial dysmorphology: increased shape variance in a mouse model for cleft lip. J Anat 212:135–143.

Presnell JK, Schreibman MP. 1997. Humason's animal tissue techniques. Baltimore: Johns Hopkins University Press.

Ruffins SW, Martin M, Keough L, Truong S, Fraser SE, Jacobs RE, Lansford R. 2007. Digital three-dimensional atlas of quail development using high-resolution MRI. ScientificWorldJournal 7:592–604.

Sharpe J. 2004. Optical projection tomography. Annu Rev Biomed Eng 6:209–228.

Stauber M, Müller R. 2008. Micro-computed tomography: a method for the nondestructive evaluation of the three-dimensional structure of biological specimens. In: Methods in molecular biology, Vol. 455. Osteoporosis: methods and protocols. Totowa, NJ: Humana Press. p 273–292.

Tyszka JM, Ewald AJ, Wallingford JB, Fraser SE. 2005. New tools for visualization and analysis of morphogenesis in spherical embryos. Dev Dyn 234:974–983.

Wanninger A. 2007. The application of confocal microscopy and 3D imaging software in functional, evolutionary, and developmental zoology: reconstructing myo- and neurogenesis in space and time. In: Méndez-Vilas A, Díaz J, editors. Modern research and educational topics in microscopy. Badajoz, Spain: FORMATEX. p 353–361.

Weninger WJ, Geyer SH, Mohun TJ, Rasskin-Gutman D, Matsui T, Ribeiro I, Costa Lda F, Izpisua-Belmonte JC, Muller GB. 2006. High-resolution episcopic microscopy: a rapid technique for high detailed 3D analysis of gene activity in the context of tissue architecture and morphology. Anat Embryol (Berl) 211: 213–221.

Vasquez SX, Hansen MS, Bahadur AN, Hockin MF, Kindlmann GL, Nevell L, Wu IQ, Grunwald DJ, Weinstein DM, Jones GM, Johnson CR, Vandeberg JL, Capecchi MR, Keller C. 2008. Optimization of volumetric computed tomography for skeletal analysis of model genetic organisms. Anat Rec (Hoboken) 291:475–487.